ISSN 1330-3651 (Print), ISSN 1848-6339 (Online)
https://doi.org/10.17559/TV-20231001000977
Original scientific paper

Analysis of Temperature-induced Deformation of Reinforced Track Slabs under the Influence of Multiple Factors

Yang LI, Luming AN, Jian ZHAO, Kailin CAO, Xianfeng SHI*

Abstract: The temperature deformation and damage of CRTS II slab track reinforced by post-installed anchors are affected by many factors, such as the state of concrete joints, and the bonding state between post-installed anchors and concrete of the track. Considering the non-linear characteristics of the mechanical properties of the concrete material, the interfacial behaviour, and the mechanical performance of the anchoring system, a finite element model of the reinforced CRTS II slab track is established to analyze the influence of multiple factors on the temperature deformation and damage behaviour of the reinforced CRTS II slab track. The results show that the main wave wavelength of the up-arching of the track slabs under temperature rise loading is smaller than the auxiliary wave wavelength, and the post-installed anchors do not significantly change the wavelengths of the main wave and the auxiliary wave. It is possible to make the longitudinal middle position of track slabs arch when anchoring reinforcement is implemented. Compared with the bonding state of anchoring reinforcement, the degree of damage of concrete joints has a greater impact on the temperature-induced deformation of the track after reinforcement. Considering the deformation of the track-slab arch, longitudinal displacement, and interlayer damage, it is recommended to repair the lower part of the concrete joints with a damage height of more than 50% of its total height in time.

Keywords: CRTS II slab track; damage behaviour; interface; post-installed reinforcement anchors; temperature-induced deformation

1 INTRODUCTION

For medium and long-distance transportation, compared with aviation, highways, and other modes of transportation, high-speed railways have advantages in terms of cost, safety, environmental protection, and so on [1-4]. Ballastless track is an important part of high-speed railway engineering. The CRTS II slab track is a typical ballastless track, which is a multi-layer composite structure system consisting of track slabs, CA mortar layer, and concrete base, or supporting layer, in which the track-slab layer consists of pre-fabricated track slabs with concrete joints cast on site. The composite structure of the track causes a discontinuity in the material strength and densification degree. Compared with the concrete base layer and CA mortar layer, the track-slab layer, which is directly exposed to the external environment is larger, and the amplitude of the temperature load changes it is subjected to is also higher. Therefore, track-slab layer diseases caused by high-temperature deformation are more common, such as arching of slabs, concrete joint breakage, etc. [5, 6]. To deal with these kinds of diseases, the post-installed anchoring method is used to connect the track slabs and concrete base, limiting the deformation of track slabs. In recent years, to prevent the diseases of tracks, post-installed anchors have been utilized in several high-speed railways.

2 LITERATURE REVIEW

Change of mechanical performance of railway tracks can be induced by repeated wheel loading, temperature change, deterioration of materials, etc.[7-10]. Samuel et al. [11] investigated the effects of railway traffic and extreme weather on the long-term performance of slab tracks. Zhou et al. [12] researched the mechanical responses of CRTS II slab tracks subject to diurnal temperature variation. Li et al. [13] studied the damage behaviour of slab tracks caused by fatigue loading. Lou et al. [14] investigated the mechanism of interfacial failure of slab tracks induced by solar radiation in alpine and plateau regions. Train-induced vibrations and noise are also one of the concerns for the performance of slab tracks [15]. Zhang et al. [16] conducted an experimental study on noise mitigation measures used for slab tracks. There is a big difference between the force-transfer mechanism of the slab tracks after post-installed reinforcement and that of the unreinforced track. At present, some studies on the force deformation and damage law of CRTS II slab track after reinforcement have been conducted. Zhong et al. [17] used the finite element simulation method to analyze the effect of post-installed anchoring on deformation of ballastless tracks during track-slab repair construction. Ren [18] established a finite element model of CRTS II slab track after anchoring reinforcement and studied the influence of the number of post-installed anchors on the arching of slab ends. Li et al. [19] used numerical simulation to study the development of the interlayer damage of post-installed anchored track. Li et al. [20] used the finite element method to study the effect of post-installed anchoring on the structural damage of the CRTS II slab track in reinforced-unreinforced transition sections. Experimental investigation and on-field tests have also been carried out to study the behaviour of the reinforced tracks. Zhao et al. [21] studied the failure mode of post-installed anchors by pull-out and shear tests. Feng et al. [22] investigated the seismic performance of CRTS II slab track reinforced by post-installed anchors by using an indoor test method. Lu et al. [23] evaluated the performance of interfaces of reinforced tracks under repeated temperature changes by experimental tests. Zhang [24] carried out on-site observation and analysis of the structural state of the CRTS II slab track after reinforcement with post-installed anchors. The above studies indicate that the serviceability of slab tracks reinforced by anchors can be significantly improved, while damage of slab tracks can still occur under complex operating conditions. As the concrete joints of CRTS II slab track are cast on-site, their strength and compactness are often lower than that of prefabricated track slabs, and it is more common for the concrete joints to be broken [25]. In addition, the waterproof adhesive of the post-installed anchoring system at the upper part of the

ballastless track is directly exposed to the atmosphere, which makes it prone to aging and breakage after being irradiated by sunlight and infiltrated by rain, resulting in the degradation of the bonding strength of the post-installed anchors and track concrete. The above factors have an important influence on the mechanical properties of CRTS II slab track reinforced by post-installed anchors, but there is a lack of relevant research at present. Therefore, this paper establishes a finite element model of the CRTS II slab track reinforced by post-installed anchors to analyze the influence law of concrete joints state and post-installed anchors state on the temperature-induced deformation of the reinforced CRTS II slab track. The insights from this study can provide theoretical guidance for the maintenance and repair of CRTS II slab tracks.

3 RESEARCH METHODOLOGY

3.1 Interfacial Constitutive Relationships and Damage Characterization

The shear and tensile tests of the interface between the track slabs and CA mortar layers (hereinafter referred to as "the interface") of the CRTS II slab track show that the relationship between the bond stress and relative displacement in the shear and tensile directions of the interface show obvious nonlinearity, i.e., the bond stress increases and then decreases with the increase of the relative displacement [26]. The relationship between bond stress and relative displacement at the interface can be characterized by the bilinear cohesive zone model shown in Fig. 1.

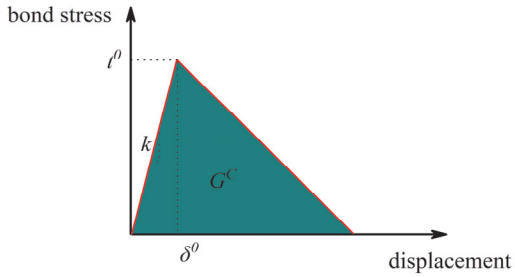

Figure 1 Bond stress-relative displacement bilinear relation

For the descending section of the bilinear relationship, the bond stress-relative displacement relationship can be expressed as:

$$\begin{cases} t_n = (1-D)\overline{t}_n, \ \overline{t}_n \geq 0 \\ t_n = \overline{t}_n, \qquad \overline{t}_n < 0 \\ t_s = (1-D)\overline{t}_s \end{cases} \tag{1}$$

In the above equation $\overline{t}_n$ and $\overline{t}_s$ are normal and tangential stresses; t_n and t_s are normal and tangential stresses after damage. When $\overline{t}_n < 0$ the normal direction is in compression, and the interface stiffness is unchanged. D is the total stiffness damage of the cohesive element, which is defined as:

$$D = \frac{\delta_m^f(\delta_m^{\max} - \delta_m^0)}{\delta_m^{\max}(\delta_m^f - \delta_m^0)} \tag{2}$$

In the above equation, $\delta_m^{\max}$ is the maximum displacement in the damage process, δ_m^0 and δ_m^f are the effective displacement when damage and fracture occur respectively. When $D = 0$, the interface is in intact state; when $D = 1$, the interface is completely debonded; when $0 < D < 1$, the interface is in a damaged state. Based on fracture mechanics theory, when the interlayer damage mode is mixed (i.e., a combination of tensile and shear forms), the Quadratic nominal stress criterion can be used as a criterion for the occurrence of damage at the interface:

$$\left\{\frac{\langle t_n \rangle}{t_n^0}\right\}^2 + \left\{\frac{t_s}{t_s^0}\right\}^2 + \left\{\frac{t_t}{t_t^0}\right\}^2 = 1 \tag{3}$$

In the above equation, t_n, t_s and t_s are the normal stress and the two tangential stresses, respectively; t_n^0, t_s^0 and t_t^0 are the bond strengths in the three directions, respectively. $\langle t_n \rangle = (t_n + |t_t|)/2$. Determination of interlayer fracture based on the energy release rate is as follows:

$$\left\{\frac{G_n}{G_n^C}\right\}^2 + \left\{\frac{G_s}{G_s^C}\right\}^2 + \left\{\frac{G_t}{G_t^C}\right\}^2 = 1 \tag{4}$$

In the above equation, G_n, G_s, and G_t are the normal and the two tangential strain energy release rates, respectively, and G_n^C, G_s^C, and G_t^C are the normal and the two tangential fracture toughness, respectively. According to reference [19], the values of cohesive zone model parameters are used, as shown in Tab. 1.

Table 1 Cohesive Zone Model Parameter

	t^0 / MPa	k / $\times 10^9$ N·m^{-3}	G^C / mJ·mm^{-2}
Normal	0,0137	0,274	0,0041
Tangents	0,01	0,2	0,003

The validation of the cohesive zone model can be found in reference [19].

3.2 Characterization of the Constitutive Relationships of Concrete Materials

Concrete materials have complex components and internal micro voids, and the emergence and expansion of microcracks will occur under external loading, which will lead to damage and deterioration of the material. The concrete damaged plasticity (CDP) model proposed by Lubliner et al. [27] and Lee et al. [28] based on the damage mechanics theory can be used to characterize the deformation and damage properties of concrete. Taking the case of uniaxial compression of concrete as an example, the material behaviour is considered to be linear-elastic at the initial stage of loading, i.e., before the stress reaches the yield stress; when the stress exceeds the yield stress, the material behaviour exhibits nonlinearity. According to the Code for the Design of Concrete Structures [29], the stress-strain relationship for concrete in uniaxial compression is:

$$\sigma_c = (1-d_c)E_0\varepsilon_c \tag{5}$$

$$d_c = \begin{cases} 1-\dfrac{\rho_c n}{n-1+x_c^{\,n}}, & |x_c \le 1 \\ 1-\dfrac{\rho_c}{\alpha_c(x_c-1)^2+x_c}, & |x_c > 1 \end{cases} \tag{6}$$

$$x_c = \frac{\varepsilon_c}{\varepsilon_{c,r}} \quad \rho_c = \frac{f_{c,r}}{E_c\varepsilon_{c,r}} \quad n = \frac{1}{1-\rho_c} \tag{7}$$

In the above equation, α_c is the value of the parameter of the descending section of the stress-strain curve during uniaxial compression, $f_{c,r}$ is the representative value of the uniaxial compressive strength of the concrete, $\varepsilon_{c,r}$ is the peak compressive strain corresponding to the representative value of the uniaxial compressive strength, and d_c is the parameter of the evolution of the compressive damage of the concrete. The CDP model is driven by inelastic strain in the finite element software, and the inelastic strain in the case of uniaxial compression of concrete can be obtained from the following equation [30]:

$$\varepsilon^{in} = \varepsilon_c - \sigma_c / E_0 \tag{8}$$

The compression damage factor expression is [30]:

$$D_c = \frac{(1-\beta_c)\varepsilon^{in}E_0}{\sigma_c + (1-\beta_c)\varepsilon^{in}E_0} \tag{9}$$

According to reference [31], β_c can be 0.6. Derivation of uniaxial tension relations for concrete can be found in References [29, 31]. Experimental validation of the concrete plasticity model can be seen in References [32].

3.3 Numerical Model of Post-installed Anchors

The slip-bond relationship between anchors and surrounding concrete is simulated by nonlinear springs in the pull-out direction (vertical direction), which connect each anchor node with the corresponding concrete node. Large-stiffness lateral springs and large-stiffness longitudinal springs are set up between the reinforcement nodes and the concrete nodes to simulate the horizontal interaction between anchors and concrete. The anchors are simulated by B33 beam elements and its material properties are simulated using a bilinear model. The slip-bond relationship between anchors and surrounding concrete established by Shu et al. [33] is used in this study, which is as follows:

$$\tau = \begin{cases} 2.68\dfrac{\tau_u}{S_u}S, & 0 \le S < S_e \\ -0.48\dfrac{\tau_u}{S_u^2}S^2 + 0.96\dfrac{\tau_u}{S_u}S + 0.52\tau_u, & S_e \le S < S_u \\ \dfrac{0.5}{S_u-5}\tau_u S + \dfrac{0.5S_u-5}{S_u-5}\tau_u, & S_u \le S < S_r \end{cases} \tag{11}$$

In the above equation, τ is the bond stress, S is the slip value, S_u is the ultimate slip, S_e is the elastic slip, and $S_e = \beta_{eu}S_u$, S_r, is the residual slip. According to Reference [19], S_u = 1.26 mm, β_{eu} = 0.28, S_r = 5 mm. τ_u is the bond strength, which is expressed as:

$$\tau_u = 5.6\alpha\sqrt{f_{cu}} / \pi \tag{12}$$

In the above equation, f_{cu} is the cubic compressive strength of concrete, α = 0.85.

3.4 Ballastless Track Model and Parameters

A finite element model has been established using the finite element modelling software ABAQUS according to the actual structure of the CRTS II slab track on viaducts, as shown in Fig. 2. Solid element C3D8R has been used to model the main track components including rails, track slabs, concrete joints, a CA mortar layer, and a concrete base. The total length of the track components corresponds to the length of a 32 m simply-supported viaduct (i.e., the length of 5 track slabs). Fixed constraints were applied to the longitudinal ends and bottom surfaces of the model. The rails, track slabs, concrete joints, CA mortar layer, and concrete base are modelled by solid elements, and the fasteners are modelled by multidirectional spring elements. The concrete strength of the track slabs and concrete joints is C55, and the concrete strength of the concrete base is C30. The Concrete Damaged Plasticity model described in section 1.2 is used to represent concrete material properties, and the parameters are shown in Reference [29]. CA mortar and rails are characterized by an elastic model, and the parameters are shown in Reference [25]. When simulating the fastener, the spring vertical stiffness is taken as 50 kN/mm, and the lateral stiffness is taken as 35 kN/mm. The longitudinal stiffness of the fasteners takes into account its nonlinear characteristics: when the relative displacement of the rail and the track slabs at the corresponding position of the fastener is less than 2 mm, the stiffness of the fastener is 4.5 kN/mm; when the relative displacement is greater than 2 mm, the longitudinal force provided by the fastener keeps as 9 kN.

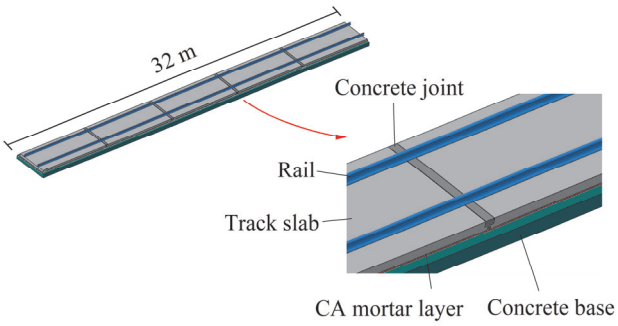

Figure 2 Finite element model

It has been found that the CA mortar is usually well bonded to the concrete base, so tie constraint is applied to the interface between the two. The interface between track slabs and CA mortar are prone to cracking, so the cohesive zone model is used to characterize the interaction between the two. Validation of the established finite element model can be found in References [19].

4 RESULTS AND DISCCUSION

In the simulation condition of this paper, the joint between the 3rd slab and the 4th slab is set as a damaged joint, and the rest of the joints are intact joints. According to the actual location of the field post-installed anchoring and the commonly used number of post-installed anchoring, each slab is reinforced by 4 rebars, as shown in Fig. 3. The maximum temperature rise of the track structure was set to 40 °C. Point A, point B, and the longitudinal path are selected as the comparative analysis location of track deformation.

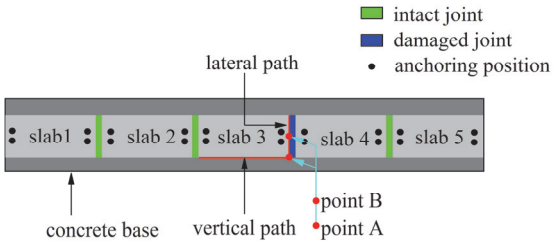

Figure 3 Working condition settings and post-installed anchoring instructions

4.1 Influence of Bonding Properties of Post-installed Anchoring Systems

To study the influence of the bonding performance of the post-installed anchoring system, this paper analyzes the deformation characteristics of the track with bond strengths of post-installed anchoring system of 2 MPa, 5 MPa, 8 MPa, 11 MPa, and without post-installed anchors. Among them, 11 MPa is the undegraded bond strength calculated by Eq. (12). According to the actual situation of concrete joint damage, it can be known that joint damage occurs mostly in narrow joints. In this paper, it is assumed that the broken height of the narrow joint is 25% of the total height of the narrow joint, and it is considered that the breakage is through the vertical direction of the track slabs, as shown in Fig. 4.

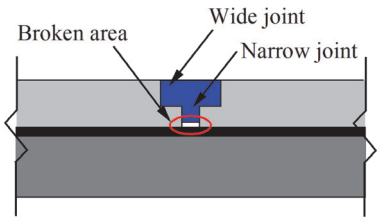

Figure 4 Schematic diagram of damaged joint

The vertical displacement of the track slab on the lateral path for different bond strengths of the post-installed anchoring system is shown in Fig. 5. From the figure, it can be seen that the two lateral ends of the track slab are slightly uplifted under the overall temperature rise load. The vertical displacement decreases after post-installed anchors are used. And with the decrease of bond strength of post-installed anchors, the vertical displacement gradually increases, but the vertical displacement after the weakening of bond strength is still significantly larger than that without post-installed anchors.

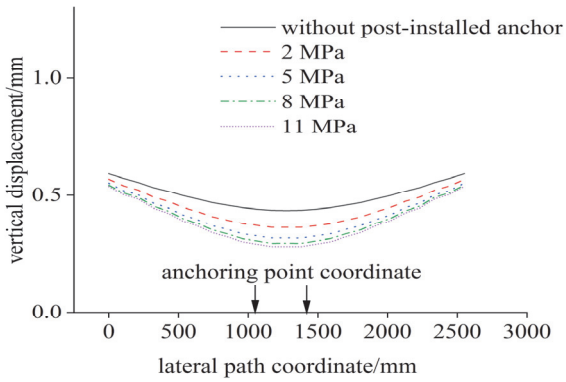

Figure 5 Effect of bond strength of post-installed anchoring system on vertical displacement in lateral path

The vertical displacement of the track slab on the longitudinal path for different bond strengths of the post-installed anchoring system is shown in Fig. 6. From the figure, it can be seen that there is a more obvious auxiliary wave in the side close to the main wave of the upper arch of the track slab, which is consistent with the theoretical analysis results of the upper arch of the ideal structure on the elastic foundation [34]. It can also be seen from Fig. 6 that the wavelength of the main wave of the upper arch of the track-slab under temperature rise loading is smaller than the wavelength of the auxiliary wave, and the post-installed anchor did not significantly change the wavelengths of the main wave and the auxiliary wave. In the main wave crest, the greater the bond strength of the post-installed anchoring system, the smaller the vertical displacement; however, the auxiliary wave crest shows the opposite trend: the greater the bond strength of the post-installed anchor, the greater the vertical displacement. The possible reason for this phenomenon is that the constraint on track displacement at the anchoring point is enhanced when the bond strength of the post-installed anchoring system is increased, which reduces the track expansion deformation that can be released by the main wave under the effect of temperature rise, and thus results in the release of greater vertical up-arching deformation of the auxiliary wave. The fixed-point restriction of the track slab using post-installed anchoring may cause a certain degree of up-arching at the location of the auxiliary wave (in the middle of the longitudinal path of the track slab), but since the main purpose of post-installed anchors is to limit the amplitude of up-arching of the main wave, this does not affect the overall effect of post-installed anchors on the prevention and control of track diseases.

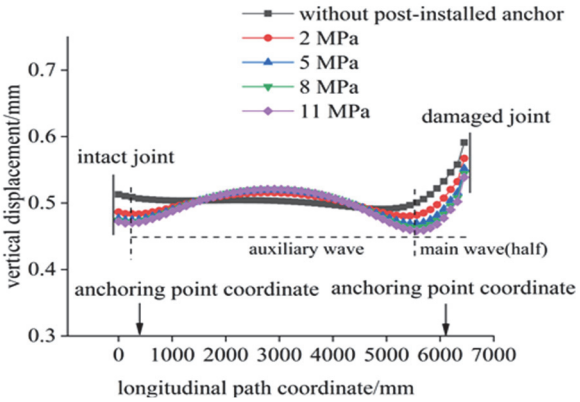

Figure 6 Effect of bond strength of post-installed anchoring system on vertical displacement of longitudinal path

Fig. 7 demonstrates the effect of the bond strength of the post-installed anchoring system on the longitudinal displacement of slabs in the longitudinal path. As can be seen from the figure, although the longitudinal displacement of the track slab has a certain degree of sudden increase at the slab-end close to the damaged joint, the maximum value of the longitudinal displacement of the track slab is small, and the track slab does not undergo overall longitudinal movement. Moreover, the difference in longitudinal displacement between the anchored and unanchored cases is not significant, which shows that the longitudinal continuity of the track slab itself can provide good longitudinal restraint for the track.

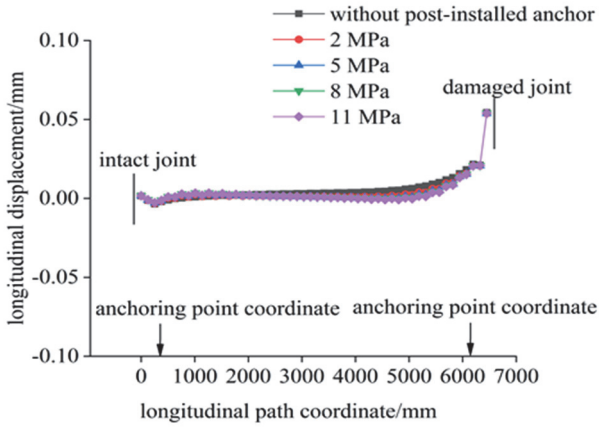

Figure 7 Effect of bond strength of post-installed anchoring system on longitudinal displacement of longitudinal path

The influence of the bond strength of the post-installed anchoring system on the interlaminar damage state of the lateral path can be seen in Fig. 8: regardless of whether post-installed anchors are set or not, the interlaminar separation occurs at both ends of the lateral path of the track slabs under the action of the maximum temperature-rise loading; however, the degree of damage to the interlaminar interface in the middle part of the lateral path is relatively small when the bond strength of post-installed anchoring system is larger.

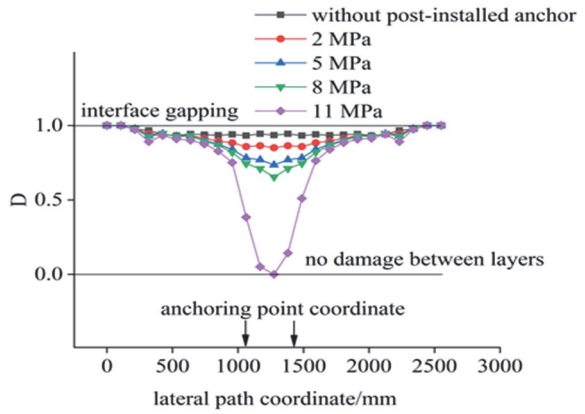

Figure 8 Effect of bond strength of post-installed anchoring system on lateral path interlayer damage value

4.2 The Effect of the Degree of Breakage of Concrete Joints

To study the influence of concrete joint breakage degree on the mechanical behaviour of ballastless track, this section analyzes the temperature deformation behaviour of the track when the breakage degree of the concrete joint is 25%, 50%, 75% and 100% respectively, where 100% indicates that the lower part of the concrete joint is completely broken. In this section, the bond strength of the post-installed anchoring system is considered as 11 MPa. The effect of the degree of concrete joint damage on the vertical displacement of track slabs in the lateral path is shown in Fig. 9. As can be seen from the figure, the larger the degree of damage of the concrete joint, the larger the vertical displacement. When the vertical displacement of the track slabs is larger, the vertical displacement of the track slabs can be regarded as the height of the gap between layers. It can be known that when the degree of breakage of the concrete joint is 100%, the height of the gap in the lateral path is more than 1.5 mm. according to the "Maintenance Rules for Ballastless Track of High-speed Railway" (TG/GW 115-2012), the CRTS II slab track with the interfacial gaps larger than 1.5 mm is the III level damage, which needs to be repaired in time.

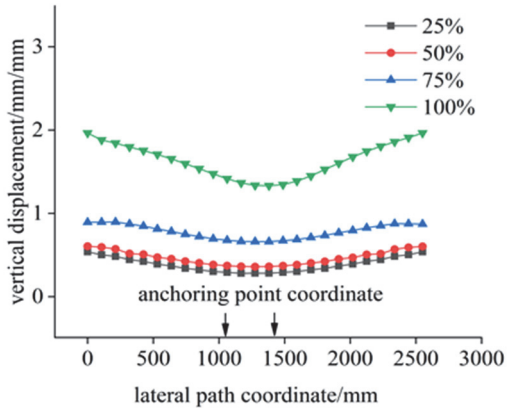

Figure 9 Effect of the degree of joint breakage on the vertical displacement of the lateral path

The effect of the degree of breakage of the concrete joint on the vertical displacement in the longitudinal path is shown in Fig. 10. From the figure, it can be seen that on the side close to the intact joint, the vertical displacement of the track slab under different degrees of concrete joint damage does not differ much, but in the side close to the damaged joint, the degree of concrete joint damage has a great influence on the vertical displacement of the track slab.

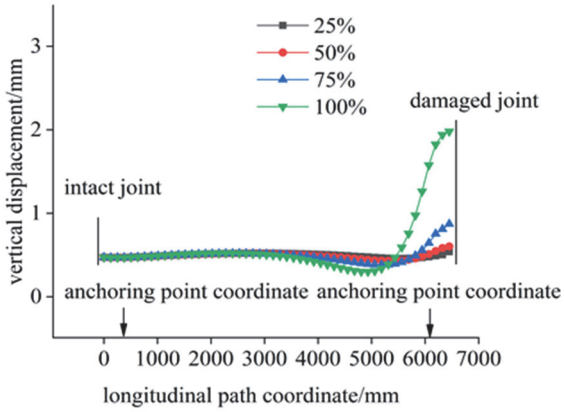

Figure 10 Effect of the degree of joint breakage on the vertical displacement of the longitudinal path

Fig. 11 shows the influence of the degree of breakage of the concrete joint on the longitudinal displacement in the longitudinal path. As can be seen from the figure, when the degree of damage to the concrete joint is less than or equal to 75%, the longitudinal displacement of the track slab is mainly concentrated on the side close to the damaged concrete joint; when the lower part of the concrete joint is completely damaged, although there are post-installed anchors, the whole track slab moves towards the damaged joint, and the maximum longitudinal displacement is more than 0.5 mm. The longitudinal movement of the track slab as a whole has an unfavorable impact on the stability of ballastless track structure, so it should be repaired in time to avoid this kind of situation.

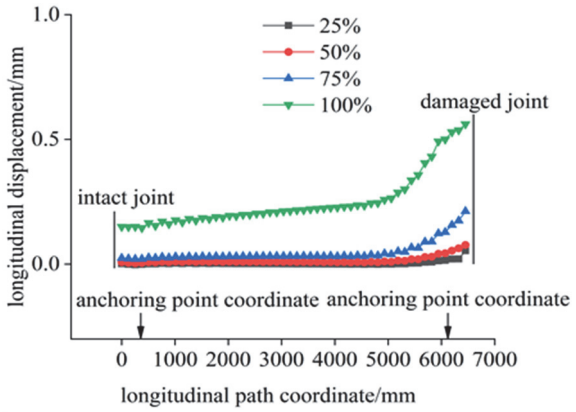

Figure 11 Effect of the degree of joint breakage on the longitudinal displacement of the longitudinal path

Fig. 12 gives the longitudinal displacement versus vertical displacement for the anchored and unanchored cases with different degrees of joint breakage. From the figure, it can be seen that the vertical displacement of the track slab is greater than the longitudinal displacement, regardless of whether the post-installed anchors are used or not. The greater the degree of damage to the concrete joint, the more obvious the effect of post-installed anchors on limiting the vertical and longitudinal displacements of the track slab. When the lower part of the concrete joint is completely damaged, the vertical displacement of the track slab without post-installed anchors is close to 4 mm, but the vertical displacement of the track slab with post-installed anchor is only about 2 mm.

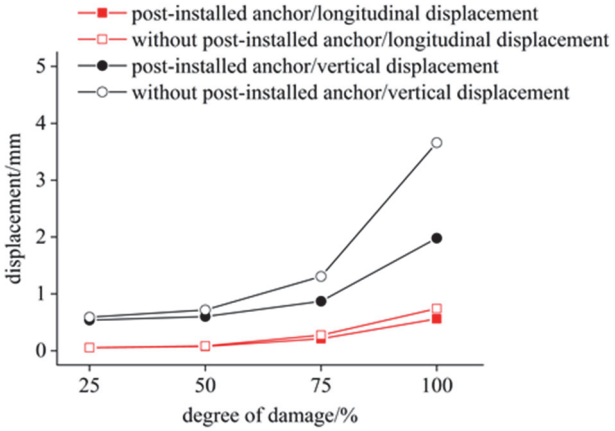

Figure 12 Effect of the degree of joint breakage on the maximum displacement

Fig. 13 shows the distribution of interlaminar damage values on the lateral path under different concrete joint breakage conditions. As can be seen from the figure, when the degree of breakage of the concrete joint is less than or equal to 50%, although interlayer damage occurs in the middle portion of the lateral path, interlayer debonding does not occur in that region. However, when the degree of damage to the concrete joints is greater than or equal to 75%, interface debonding does occur across the entire lateral path.

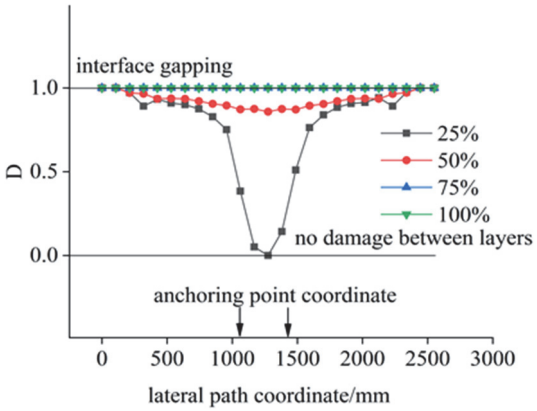

Figure 13 Effect of the degree of joint breakage on the value of interlayer damage

4.3 The Combined Effect of Concrete Joint Breakage and the Bonding State of the Post-installed Anchors

From the above research results, it is known that the bonding state of post-installed anchors and the damage state of the concrete joint have a certain influence on the temperature deformation of the ballastless track after reinforcement. In this section, the temperature deformation of the ballastless track under the combinations of different parameters is investigated by taking the bonding strength of post-installed anchors and the degree of damage of concrete joints as the basic parameters. The maximum vertical displacement distribution of the track slab under the various working conditions is shown in Fig. 14. It can be seen from the figure that when the bond strength of the post-installed anchors is a certain value, the maximum vertical displacement increases with the increase of the damage degree of the concrete joint; when the damage degree of the concrete joint is a certain value, the maximum vertical displacement decreases with the increase of the strength of the post-installed anchors. However, the effect of the increase in post-installed anchor strength on limiting the increasing trend of vertical displacement is small, while the degree of damage to the concrete joint has a greater impact on the change of vertical displacement. When the damage degree of the concrete joint is less than 75%, the vertical upward arch of the track slab can be controlled within 1.5 mm. When the damage degree of the concrete joint is less than 60%, the vertical displacement of the track-slab can be controlled within 1 mm (corresponding to the II level gap stipulated in the "Maintenance Rules for Ballastless Track of High-speed Railway" (TG/GW 115-2012).

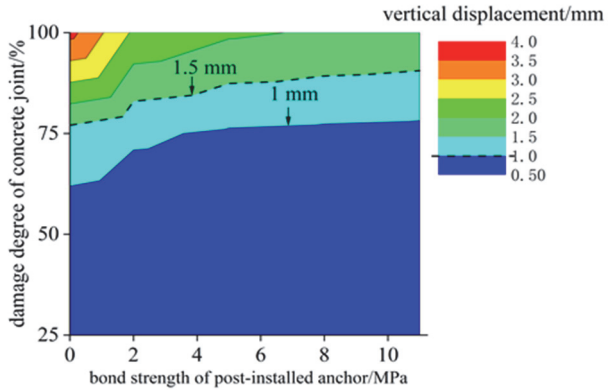

Figure 14 Distribution of maximum vertical displacement of track-slab under multifactorial action

The maximum longitudinal displacement distribution of the track slab under the different working conditions is shown in Fig. 15, from which it can be seen that when the bond strength of the post-installed anchors is a certain value, the maximum longitudinal displacement increases with the increase in the degree of damage of the concrete joint; when the degree of breakage of the concrete joint is a certain value, the maximum longitudinal displacement decreases with the increase in the bond strength of the post-installed anchoring system. The effect of increasing the bond strength of the post-installed anchoring system on limiting the trend of increasing longitudinal displacement is small, and the degree of breakage of the concrete joint plays a significant role in controlling the change of longitudinal displacement. When the damage degree of the concrete joint is less than 50%, the longitudinal displacement of the track-slab is less than 0.1 mm.

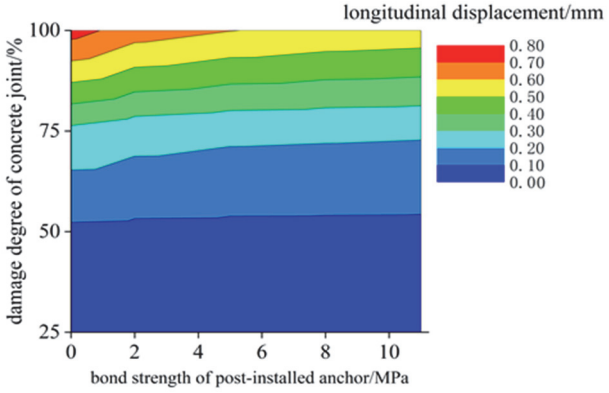

Figure 15 Distribution of maximum longitudinal displacement of track-slab under multifactorial action

The temperature increase value at which the interfacial damage value reaches 1 at a certain point on the interface between the track slab and the CA mortar layer is defined as the critical temperature rise for that point. The higher the critical temperature rise value, the less likely debonding to occur at the interface. From Fig. 16a, it can be seen that at point A, when bond strength of the post-installed anchoring system is a certain value, the critical temperature rise increases with the increase of the damage degree of the concrete joint; when the damage degree of the concrete joint is a certain value, the critical temperature rise decreases with the increase of the bond strength of the post-installed anchoring system. The increase of post-installed anchor bond strength has less effect on slowing down the increasing trend of critical temperature rise, and the degree of breakage of the concrete joint has a significant effect on controlling the change of critical temperature rise. As can be seen from Fig. 16b, the trend of change of critical temperature rise at point B is basically the same as that at point A. However, the difference is that the critical temperature rise at point A is lower than that at point B under different parameter combinations. From Fig. 16b, it can be found that when the degree of breakage of the concrete joint is less than 50%, whether the post-installed anchors are used or not, the critical temperature at point B is higher than 40 °C, which indicates that under the normal temperature rise loading conditions, the degree of breakage of the concrete joint should be less than 50% to ensure that debonding will not occur in the lateral center of the track-slab. In order to detect the anchorage system degradation or joint damage for timely maintenance, in addition to manual inspections and track inspection car, new detection methods aided by machine learning techniques should be used [35]. It can be found that the critical temperature rise increases with the increase of the damage degree of the concrete joint. For a severe damage scenario in which the degree of breakage of the concrete joint is over 75%, the critical temperature rise is about 30 °C. Therefore, it is recommended to increase the frequency of inspection to detect the interface degradation in time when the temperature rises over 30 °C.

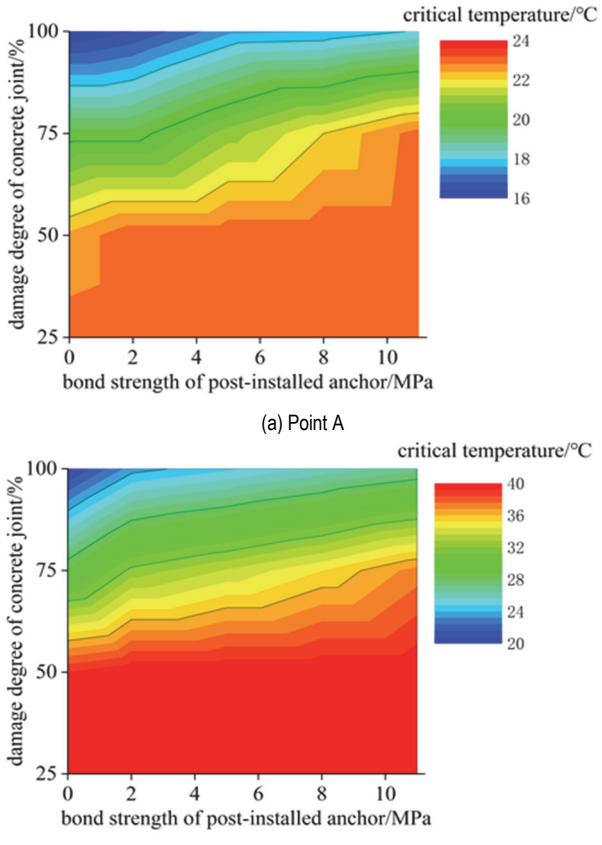

Figure 16 Critical temperature rise distribution under multifactorial effects

5 CONCLUSIONS

(1) The wavelength of the main wave of the arch on the track slabs under temperature rise loading is smaller

than the wavelength of the auxiliary wave, and the post-installed anchors do not significantly change the wavelengths of the main and auxiliary waves.

(2) Limiting the displacement of the track slab using post-installed anchoring has the potential to cause some degree of upward arching at the mid-longitudinal position of the track slab. Therefore, anchors should also be installed at the mid-longitudinal position of the track slab.

(3) The greater the degree of breakage of the concrete joint, the more pronounced the effect of the post-installed anchors on limiting the vertical and longitudinal displacements of the track slab. Therefore, concrete materials with high toughness are suggested to be selected for concrete joint to improve the mechanical performance of the slab track.

(4) Compared with the bond state of the post-installed anchor, the degree of breakage of the concrete joint has a greater impact on the temperature-induced deformation of the ballastless track after reinforcement. Considering the deformation of the track-slab and interlayer damage, it is recommended to repair the lower part of the concrete joints with a damage height of more than 50% of its height in time.

(5) For a severe damage scenario in which the degree of breakage of the concrete joint is over 75%, the critical temperature rise is about 30 °C. Therefore, it is recommended to increase the frequency of inspection to detect the interface degradation in time when the temperature rises over 30 °C.

It should be mentioned that some other factors including rail pad stiffness and CA mortar properties may also have some minor influence on the deformation of reinforced slab tracks. In addition, combined action of cyclic thermal loading with dynamic train loads can be closer to real field conditions. In the future, the effects of other factors on mechanical properties of reinforced slab tracks subjected to the combined action of cyclic thermal loading with dynamic train loads should be studied. Besides, spatial variability and uncertainty in material parameters may affect the deformation of the reinforced tracks, which should also be considered in future works.

6 REFERENCES

[1] Rungskunroch, P., Shen, Z., & Kaewunruen, S. (2021). Benchmarking environmental and economic impacts from the HSR networks considering life cycle perspectives. *Environmental Impact Assessment Review,* 90, 106608. https://doi.org/10.1016/j.eiar.2021.106608

[2] Yang, Y., Yin, Y. X., Wang, Y. P., Meng, R., & Yuan, Z. (2023). Modeling of freeway real-time traffic crash risk based on dynamic traffic flow considering temporal effect difference. *Journal of Transportation Engineering Part A Systems, 149*(7), 04023063. https://doi.org/10.1061/JTEPBS.TEENG-7717

[3] Yuan, Z., Yuan, X., Yang, Y., Chen, Y., Nie, Y., Cao, M., & Chen, L. (2023). Greenhouse gas emission analysis and measurement for urban rail transit: a review of research progress and prospects. *Digital Transportation and Safety, 1*(1), 37-52. https://doi.org/10.48130/DTS-2023-0004

[4] Yang,Y., Tian, N., Wang, Y., & Yuan, Z. (2022). A parallel FP-growth mining algorithm with load balancing constraints for traffic crash data. *International Journal of Computers Communications & Control, 17*(4), 4806. https://doi.org/10.15837/ijccc.2022.4.4806

[5] Li, Y., Li, H., Zhang, G., & Kaewunruen, S. (2023). Nonlinear responses of longitudinally coupled slab tracks exposed to extreme heat waves. *Engineering Structures, 281*, 115789. https://doi.org/10.1016/j.engstruct.2023.115789

[6] Ren, J., Liu, W., Du, W., Zheng, J., Wei, H., Zhang, K., & Ye, W. (2023). Identification method for subgrade settlement of ballastless track based on vehicle vibration signals and machine learning. *Construction and Building Materials, 369*, 130573. https://doi.org/10.1016/j.conbuildmat.2023.130573

[7] Zhou, R., Yang, P., Li, Y., Tao, Y. G., Xu, J., & Zhu, Z. (2023). Interfacial properties of double-block ballastless track under various environmental conditions. *International Journal of Mechanical Sciences, 266*, 108954. https://doi.org/10.1016/j.ijmecsci.2023.108954

[8] Zhang, Y., Gao, L., Cai, X., Li, Q., & Kong, X. (2020). Influences of triethanolamine on the performance of cement pastes used in slab track. *Construction and Building Materials, 238*, 117670 https://doi.org/10.1016/j.conbuildmat.2019.117670

[9] Zhang, Y., Wu, K., Cai, X., Gao, L., Wang, K., & Zhang, X. (2022). Numerical study on the pipe flow characteristics of grouting repairing pastes used in slab track. *Construction and Building Materials, 320*, 126214. https://doi.org/10.1016/j.conbuildmat.2021.126214

[10] Fu, H., Yang, Y., & Kaewunruen, S. (2023). Multi-hazard effects of crosswinds on cascading failures of conventional and interspersed railway tracks exposed to ballast washaway and moving train loads. *Sensors, 23*(4), 1786. https://doi.org/10.3390/s23041786

[11] Samuel, R. M. & Patrícia, A. F. (2022). The role of railway traffic and extreme weather on slab track long-term performance. *Construction and Building Materials, 322*, 126445. https://doi.org/10.1016/j.conbuildmat.2022.126445

[12] Zhou, R., Zhu, X., Du, Y., Ma, C., Liu, W., Ren, W., & Zhang, L. (2023). Thermal response of the bridge supported longitudinal CRTS II slab track subject to diurnal temperature variation. *Construction and Building Materials, 395*, 132332. https://doi.org/10.1016/j.conbuildmat.2023.132332

[13] Li. Z., Li. Z., Huang. W., Thang, H., & Zhang, H. (2022). Fatigue damage analysis of ballastless slab track in heavy-haul railway tunnels. *Underground Space, 7*, 440-452. https://doi.org/10.1016/j.undsp.2021.10.003

[14] Lou, P. & Shi, T. (2023). Thermal arching and interfacial damage evolutionof CRTS-II slab track under solar radiation inalpine and plateau regions. *Alexandria Engineering Journal, 74*, 301-315. https://doi.org/10.1016/j.aej.2023.05.032

[15] Liang, R., Liu, W., Li, C., Li, W., & Wu, Z. (2023). A novel efficient probabilistic prediction approach for train-induced ground vibrations based on transfer learning, *Journal of Vibration and Control*. https://doi.org/10.1177/10775463221148792

[16] Zhang, X., Jeong, H., Thompson, D., & Squicciarini, G. (2023). Experimental study of noise mitigation measures on a slab track. *Applied Acoustics, 172*, 107630. https://doi.org/10.1016/j.apacoust.2020.107630

[17] Zhong, Y., Gao, L., & Hou, B. (2018). Shear Behavior of Mortar Layer in Continuous Slab Track with Different Arrangement Schemes of Embedded Steel Bars. *Journal of Southwest Jiaotong University, 53*(1), 38-45.

[18] Ren, X. (2019). *Research on upwarp of CRTS II ballastless track slab end and its renovation*. Beijing: Beijing Jiaotong University.

[19] Li, Y., Chen, J., Wang, J., Shi, X., & Wang, R.. (2021). Interfacial failure and arching of the CRTS II slab track reinforced by post-installed reinforcement bars due to thermal effects. *Engineering Failure Analysis, 125*, 105405. https://doi.org/10.1016/j.engfailanal.2021.105405

[20] Li, Y., Li,H., Zhou, R., Chen, J., Song, Y., & Cao, K. (2024). Mechanical performance of CRTS II slab tracks in

reinforced-unreinforced transition zone in extreme heat events. *Transportation Geotechnics, 45*, 101201. https://doi.org/10.1016/j.trgeo.2024.101201
[21] Zhao, H., Sun, L., Li, Q., & et al. (2022). Experimental study on mechanical properties of bonded rebars in continuous slab ballastless track of high-speed railway. *Journal of the China Railway Society, 44*(7), 92-97.
[22] Feng, Y., Jiang, L., Zhou, W., Han, J., Zhang, Y., Nie, L., Tan, Z., & Liu, X. (2022). Experimental investigation on shear steel bars in CRTS II slab ballastless track under low-cyclic reciprocating load. *Construction and Building Materials, 255*, 119425. https://doi.org/10.1016/j.conbuildmat.2020.119425
[23] Lu, H., & Xu, Y. (2023). Evolution of interface performance of longitudinal ballastless track under temperature load after embedded steel bars. *Journal of South China University of Technology (Natural Science Edition), 51*(8), 21-31.
[24] Zhang, J. (2018). Research on Slab Expansion Mechanism and Treatment Measures for CRTS II Slab Ballastless Track. *Railway Engineering, 58*(7), 104-107.
[25] Li, Y., Chen, J., Wang, J., Shi, X., & Chen, L. (2020). Analysis of damage of joints in CRTSII slab track under temperature and vehicle loads. *KSCE Journal of Civil Engineering, 24*(4), 1209-1218. https://doi.org/10.1007/s12205-020-1799-y
[26] Xu, Y., Yan, D., Zhu, W., & Zhou, Y. (2020). Study on the mechanical performance and interface damage of CRTS II slab track with debonding repairment. *Construction and Building Materials, 257*, 119600. https://doi.org/10.1016/j.conbuildmat.2020.119600
[27] Lubliner, J., Oliver, J., Oller, S., & Oñate, E. (1989). A plastic damage model for concrete. *International Journal of Solids and Structures, 25*(3), 299-326. https://doi.org/10.1016/0020-7683(89)90050-4
[28] Lee, J. & Fenves, G. (1998). Plastic-damage model for cyclic loading of concrete structures. *Journal of Engineering Mechanics, 124*(8), 892-900. https://doi.org/10.1061/(ASCE)0733-9399(1998)124:8(892)
[29] Ministry of Housing and Urban-Rural Development of the People's Republic of China. (2014). *Code for design of concrete structures: GB 50010-2010*. Beijing: China Architecture & Building Press.
[30] Zhang, J., Wang, Q., & et al. (2008). Parameters Verification of Concrete Damaged Plastic Model of ABAQUS. *Building Structure, 8*, 127-130.
[31] Ren, J., Wang, J., Li, J., & et al. (2019). Damage law of track slab based on concrete damaged plasticity model. *Journal of Zhejiang University (Engineering Science), 53*(8), 1448-1456.
[32] Cai, X., Zhong, Y., Ruan, Q., & et al. (2019). Application of concrete damaged plasticity model to nonlinear analysis of ballastless track. *Journal of the China Railway Society, 41*(5), 109-118.
[33] Shu, R., Zhang, J., & Zhang, C. (2008). Analysis on bond-slip performance and load transfer mechanism of bonded rebars. *Structural Engineers, 5*, 64-70.
[34] Liu, X., Liu, X., Xiao, J., & et al. (2018). Vertical stability of longitudinal continuous ballastless track under temperature variation. *Journal of Southwest JiaotongUniversity, 53*(5), 921-927.
[35] Cai, X., Tang, X., Pan, S., Wang, Y., Yan, H., Ren, Y., Chen, N., & Hou, Y. (2023). Intelligent recognition of defects inhigh-speed railway slab track with limited dataset. *Computer-Aided Civil and Infrastructure Engineering*, 1-18. https://doi.org/10.1111/mice.13109

Contact information:

Yang LI, PhD, Lecturer
State Key Laboratory of Mechanical Behavior and System Safety of Traffic, Engineering Structures & Key Laboratory of Roads and Railway Engineering, Safety Control,
Ministry of Education,
Shijiazhuang Tiedao University,
Shijiazhuang, Hebei, China, 050043
E-mail: lyang1@stdu.edu.cn

Luming AN, Master Engineer
China Railway Construction Bridge Engineering Bureau Group CO., LTD,
Tianjin, China, 300300
E-mail:anluming@foxmail.com

Jian ZHAO, PhD, Senior Engineer
China Railway Construction Bridge Engineering Bureau Group CO., LTD,
Tianjin, China, 300300
E-mail: zhaojianll@126.com

Kailin CAO, Master Candidate
State Key Laboratory of Mechanical Behavior and System Safety of Traffic, Engineering Structures,
Ministry of Education,
Shijiazhuang Tiedao University,
Shijiazhuang, Hebei, China, 050043
E-mail: 1542697291@qq.com

Xianfeng SHI, PhD, Professor
(Corresponding author)
State Key Laboratory of Mechanical Behavior and System Safety of Traffic, Engineering Structures,
Ministry of Education,
Shijiazhuang Tiedao University,
Shijiazhuang, Hebei, China, 050043
E-mail: 270192224@qq.com